# Micrometeorology

Bearbeitet von
Thomas Foken, Carmen J Nappo

1. Auflage 2008. Taschenbuch. xx, 308 S. Paperback
ISBN 978 3 540 74665 2
Format (B x L): 15,5 x 23,5 cm
Gewicht: 1020 g

# 1 General Basics

This introductory chapter gives the basics for this book, and terms such as micrometeorology, atmospheric boundary layer, and meteorological scales are defined and presented in relation to the subject matter of this book. Besides an historical outline, the energy and water balance equations at the Earth's surface and the transport processes are discussed. The micrometeorological basics are given, which will be advanced in the following theoretical and experimental chapters.

## 1.1 Micrometeorology

Meteorology is one of the oldest sciences in the world. It can be traced back to Aristotle (384–322 BCE), who wrote the four volumes of the book *Meteorology*. In ancient times, appearances in the air were called meteors. In the first half of the 20th century, the upper soil layers were considered part of meteorology (Hann and Süring 1939). Today meteorology is understood in a very general sense to be the science of the atmosphere (Dutton 2002; Glickman 2000; Kraus 2004), and includes also the mean states (climatology). Sometimes the definition of meteorology is very narrow, and only related to the physics of the atmosphere or weather prediction. To understand atmospheric processes, many other sciences such as physics, chemistry, biology and all geosciences are necessary, and it is not easy to find the boundaries of these disciplines. In a pragmatic way, meteorology is related only to processes that take place *in-situ* in the atmosphere, while other sciences can investigate processes and reactions in the laboratory. This underlines the specific character of meteorology, *i.e.*, a science that investigates an open system with a great number of atmospheric influences operating at all times but with changing intensity. Meteorology is subdivided into branches (Glickman 2000; Houghton 1985; Hupfer and Kuttler 2005; Kraus 2004). The main branches are theoretical meteorology, observational meteorology, and applied meteorology. Applied meteorology includes weather prediction and climatology. Climatology must be seen in a much wider geosciences context. The subdivision is continued up to special areas of investigation such as maritime meteorology.

The applications of time and space scales became popular over the last 50 years, and subdivisions into macro-, meso- and micrometeorology were developed. Micrometeorology is not restricted to particular processes, but to the time and space scales of these processes (see Chap. 1.2). The significance of micrometeorology is in this limitation. The living environment of mankind is the main object of micrometeorological research. This is the atmospheric surface layer, the lowest 5–10% of the atmospheric boundary layer, which ranges in depth from about 0.5 to 2 km.

The surface layer is one of the main energy-exchange layers of the atmosphere, and accordingly the transformations of solar energy into other forms of energy are a main subject of micrometeorology. Furthermore, the surface layer is a source of friction, which causes a dramatic modification of the wind field and the exchange processes between the Earth's surface and the free troposphere. Due to the coupling of time and space scales in the atmosphere, the relevant time scale of micrometeorology is less than the diurnal cycle. A recent definition of micrometeorology is (Glickman 2000):

> Micrometeorology is a part of meteorology that deals with observations and processes in the smaller scales of time and space, approximately smaller than 1 km and one day. Micrometeorological processes are limited to shallow layers with frictional influence (slightly larger phenomena such as convective thermals are not part of micrometeorology). Therefore, the subject of micrometeorology is the bottom of the atmospheric boundary layer, namely, the surface layer. Exchange processes of energy, gases, *etc.*, between the atmosphere and the underlying surface (water, soil, plants) are important topics. Microclimatology describes the time-averaged (long-term) micrometeorological processes while the micrometeorologist is interested in their fluctuations.

If one examines the areas of investigation of applied meteorology (Fig. 1.1) it will be apparent that the main topics are related to microscale processes. Therefore, we see that micrometeorology gives the theoretical, experimental, and climatological basis for most of the applied parts of meteorology, which are related to the surface layer and the atmospheric boundary layer. Also, recent definitions such as environmental meteorology are related to micrometeorology. Applied meteorology often includes weather prediction and the study of air pollution.

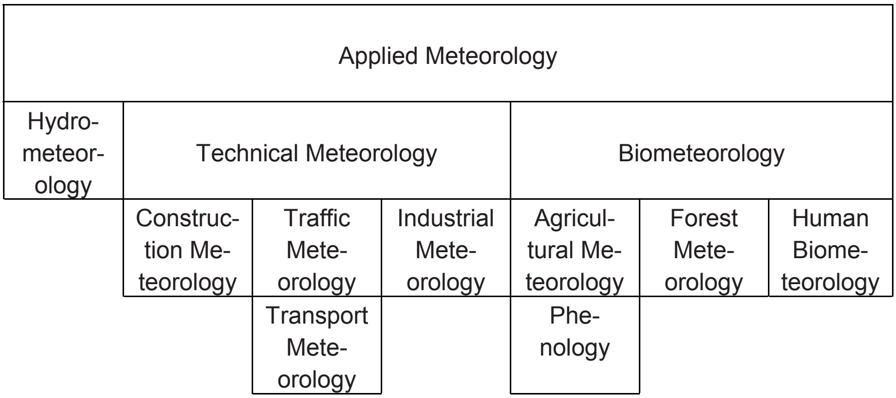


**Fig. 1.1.** Classification of applied meteorology

The basics of micrometeorology come from hydrodynamics. The following historical remarks are based on papers by Lumley and Yaglom (2001) and Foken (2006a). The origin may be dated to the year 1895, when Reynolds (1894) defined the averaging of turbulent processes, and described the equation of turbulent energy. Further steps were the mixing length approach by Taylor (1915) and Prandtl (1925), and the consideration of buoyancy effects by Richardson (1920). The every-day used term "turbulence element" is based on Barkov (1914), who found these in wind observations analyzed during a long stay in winter in the Antarctic ice shield. The actual term *micrometeorology* is dated to the determination of energy and matter exchange and the formulation of the *Austausch coefficient* by Schmidt (1925) in Vienna. At the same time in Munich, Geiger (1927) summarized microclimatological works in his famous book *The Climate near the Ground*, which is still in print (Geiger *et al.* 1995). The experimental and climatological application of these investigations of turbulent exchange processes were done mainly by Albrecht (1940) in Potsdam, who also wrote parts of the classical textbook by Kleinschmidt (1935) on meteorological instruments. In Leipzig, Lettau (1939) investigated the atmospheric boundary layer and continued his investigation after the Second World War in the U.S.A. (Lettau and Davidson 1957). With the end of the Second World War, an era of more than 20 years of famous German-speaking micrometeorological scientists ended, but the word *Austausch coefficient* was maintained from that period.

The origin of modern turbulence research in micrometeorology was in the 1940s in Russia. Following the fundamental studies on isotropic turbulence and the turbulence spectra by Kármán and Howardt (1938) and Taylor (1938), Kolmogorov (1941a, b) gave theoretical reasons for the turbulence spectra. In 1943, Obukhov (published in 1946), found a scaling parameter that connects all near-surface turbulence processes. This paper (Obukhov 1971) was so important because of its relevance to micrometeorology, it was once again published by Businger and Yaglom (1971). A similar paper was published by Lettau (1949), but was not applied because it used a different scaling. Using what became known as *similarity theory*, Monin and Obukhov (1954) created the basics of the modern stability-dependent determination of the exchange process. At the same time, a direct method to measure turbulent fluxes was developed (Montgomery 1948; Obukhov 1951; Swinbank 1951), which has become known as the *eddy-covariance* method. This method became truly established only after the development of the sonic anemometer, for which the basic equations were given by Schotland (1955). Following the development of a sonic thermometer by Barrett and Suomi (1949), a vertical sonic anemometer with 1m path length (Suomi 1957) was used in the O'Neill experiment in 1953 (Lettau and Davidson 1957). The design of today's anemometers was first developed by Bovscheverov and Voronov (1960), and later improved by Kaimal and Businger (1963) and Mitsuta (1966). The first anemometers used the phase shift between the transmitted and the received signal. The latter anemometers measured the time difference of the the running time along the path in both directions between the transmitted and received signal, and recent anemometers measure the time directly (Hanafusa *et al.* 1982). Following the early work by Sheppard (1947), the surface stress was directly measured with a drag plate in Australia (Bradley 1968b), and the sensible and latent heat fluxes were measured with highly sensitive modified classical sensors (Dyer *et al.* 1967).

These findings formed the basis for many famous experiments (see Appendix A5). Among them were the many prominent Australian experiments for studying turbulent exchange processes (Garratt and Hicks 1990). These were the so-called intercomparison experiments for turbulence sensors (Dyer *et al.* 1982; Miyake *et al.* 1971; Tsvang *et al.* 1973, 1985). Present day investigations are based mainly on the *KANSAS 1968* experiment (Izumi 1971; Kaimal and Wyngaard 1990). That experiment became the basis for the formulation of the universal functions (Businger *et al.* 1971) and the turbulence energy equation (Wyngaard *et al.* 1971a), which were based on an obscure earlier paper by Obukhov (1960). Twenty years after the issue of the first textbook on micrometeorology by Sutton (1953), an important state-of-the-art summary of turbulent exchange between the lower atmosphere and the surface was given in 1973 at the *Workshop on Micrometeorology* (Haugen 1973).

After some criticism of the experimental design of the KANSAS experiment by Wieringa (1980), and the reply by Wyngaard *et al.* (1982), who recommended a repetition of the experiment, several micrometeorological experiments were conducted, including investigations of fundamental micrometeorological issues, for example the Swedish experiments at Lövsta (Högström 1990). Finally, the corrected universal functions by Högström (1988) comprise our most current knowledge.

At the end of the 1980s, the step to micrometeorological experiments in heterogeneous terrain became possible. At about the same time, similar experiments were conducted in the U.S.A. (FIFE, Sellers *et al.* 1988), in France (HAPEX, André *et al.* 1990) and in Russia (KUREX, Tsvang *et al.* 1991). These experiments were to become the bases of many further experiments (see Appendix A5).

During the last 30 years, there were many of updates and increases in precision in the experimental and theoretical fields, but significant new results in problems such as heterogeneous surfaces and stable stratifications are still missing.

## 1.2 Atmospheric Scales

Contrary to other geophysical processes, meteorological processes have a clear time-space scaling (Beniston 1998). The reason for this is the spectral organization of atmospheric processes, where relevant wavelengths (extensions) are related to distinct durations in time (frequencies). The largest wavelengths are those of atmospheric circulation systems with 3–6 days duration and an extension of some thousands of kilometers (Rossby waves). The daily cycle is a prominent frequency. The time interval from minutes to seconds is characterized by exchange processes of energy and matter in the range of the so-called micro-turbulence, a main topic of micrometeorological investigations (see Chap. 1.4.3). The principle of classification was formulated by Orlanski (1975), see Fig. 1.2a. While atmospheric processes are strictly organized, the hydrological processes in soils and plant ecosystems have for the same time scales significantly smaller space scales. For example, in the case of coupling hydrologic with atmospheric models one must develop strategies to transfer hydrologic processes to the larger atmospheric space scale (Fig. 1.2b).

Different scale definitions in different scientific disciplines create problems in interdisciplinary communications. In addition, in climatology textbooks different scale concepts are discussed which are not easily comparable with the very clear meteorological scale concepts (see Chap. 7.1).

Because weather phenomena are classified according to space-time scales, the space-time scales of climate and weather prediction models must be classified in a similar way. For example, large-scale circulation models are assigned to the macro-β range. The classical weather forecast was formally related to the meso-α range, but with today's high-resolution models they are related to the meso-β,γ scale. Micrometeorology is related to all micro-scales and also partly to the meso-γ scale.

This scaling principle is basic for measurements of atmospheric processes. For instance, to measure the spatial extension of a small low-pressure system, high-resolution (small scale) measurements are necessary. The same is true for the movement of systems. The frequency of these measurements must be related to the velocity of the pressure system. This is valid for all scales, and phenomena can only be observed if the measurements are made on smaller space and time scales. Therefore, the sampling theorem (see Chap. 6.1.2) is of prime importance for all meteorological measurements and scales.

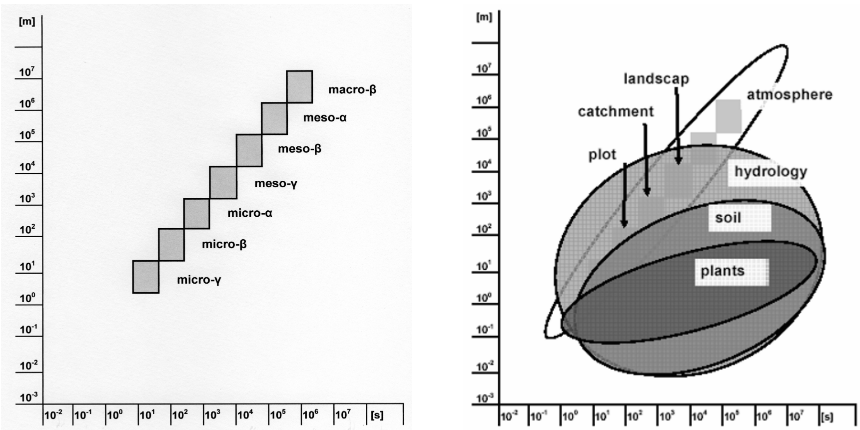


**Fig. 1.2.** (**a**) Scales of atmospheric processes according to Orlanski (1975); (**b**) Atmospheric scales added by typical scales in hydrology (Blöschl and Sivapalan 1995), in soils (Vogel and Roth 2003) and in plant ecosystems (Schoonmaker 1998)

## 1.3 Atmospheric Boundary Layer

The atmospheric boundary layer is the lowest part of the troposphere near the ground where the friction stress decreases with height. The wind velocity decreases significantly from its geostrophic value above the boundary layer to the wind near the surface, and the wind direction changes counter-clockwise up to 30–45° in the Northern hemisphere. In addition, thermal properties influence the boundary layer. Frequently the synonym *planetary boundary layer* is used in theoretical meteorology, where the general regularities of the boundary layers of planetary atmospheres are investigated. Above the boundary layer, lays a mostly statically-stable layer (inversion) with intermittent turbulence. The exchange processes between the atmospheric boundary layer and the troposphere take place in the entrainment zone. The thickness of this layer is approximately 10% of the atmospheric boundary layer, which has a thickness of about 1–2 km over land and 0.5 km over the oceans. For strong stable stratification, its thickness can be about 10 m or less.

The daily cycle is highly variable (Stull 1988), see Fig. 1.3. After sunrise, the atmosphere is warmed by the turbulent heat flux from the ground surface, and the inversion layer formed during the night brakes up. The new layer is very turbulent, well mixed (mixed layer), and bounded above by an entrainment zone. Shortly before sunset, the stable (night time) boundary layer develops near the ground. This stable layer has the character of a surface inversion and is only some 100 m deep. Above this layer, the mixed layer of the day is now much less turbulent. It is called the residual-layer, and is capped by a free (capping) inversion – the upper border of the boundary layer (Seibert *et al.* 2000). After sunrise, the developing mixed layer quickly destroys the stable boundary layer and the residual layer. On cloudy days and in winter, when the solar radiation and the energy transport to the surface are weak, the mixed layer will not disturb the residual layer, and the boundary layer is generally stratified. On days with strong solar radiation, the boundary layer structure will be destroyed by convective cells, which develop some 10 m above the ground. These cells have relatively small upwind cells relatively high vertical wind speeds, and typically develop over large areas with uniform surface heating. This is according to model studies over areas which are larger than 200–500 m$^2$ (Shen and Leclerc 1995).

In the upper part of the atmospheric boundary layer (upper layer or Ekman layer), the changes of the wind direction take place. The lowest 10% is called the surface or Prandtl layer (Fig. 1.4). Its height is approximately 20–50 m in the case of unstable stratification and a few meters for stable stratification. It is also called the *constant flux layer* because of the assumption of constant fluxes with height within the layer. This offers the possibility to estimate, for example, the fluxes of sensible and latent heat in this layer while in the upper layers flux divergences dominate. The atmospheric boundary layer is turbulent to a large degree, and only within a few millimeters above the surface do the molecular exchange processes dominate. Because the turbulent processes are about $10^5$ fold more effective than molecular processes and because of the assumption of a constant flux, the linear vertical gradients of properties very near the surface must be very large. For example, temperature gradients up to $10^3$ $Km^{-1}$ have been measured (Fig. 1.5). Between this molecular boundary layer (term used for scalars) or laminar boundary layer (term used for the flow field) and the turbulent layer, a viscous sublayer (buffer layer) exists with mixed exchange conditions and a thickness of about 1 cm. According to the similarity theory of Monin and Obukhov (1954), a layer with a thickness of approximately 1 m (dynamical sublayer) is not influenced by the atmospheric stability – this layer is nearly neutral all of the time.

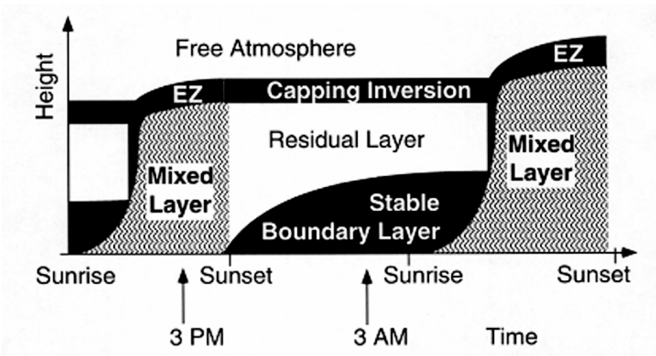


**Fig. 1.3.** Daily cycle of the structure of the atmospheric boundary layer (Stull 2000), EZ: Entrainment zone

<table>
<tr><th>height in m</th><th colspan="2">name</th><th colspan="2">exchange</th><th>stability</th></tr>
<tr><td>1000</td><td colspan="2">upper layer (Ekman-layer)</td><td rowspan="3">turbulent</td><td>no const. flux</td><td rowspan="2">influence of stability</td></tr>
<tr><td>20</td><td>turbulent layer</td><td rowspan="4">surface layer (Prandtl-layer)</td><td rowspan="4">flux constant with height</td></tr>
<tr><td>1</td><td>dynamical sublayer</td><td rowspan="3">no influence of stability</td></tr>
<tr><td>0.01</td><td>viscous sublayer</td><td>molecular/ turbulent</td></tr>
<tr><td>0.001</td><td>laminar boundary layer</td><td>molecular</td></tr>
</table>

**Fig. 1.4.** Structure of the atmospheric boundary layer

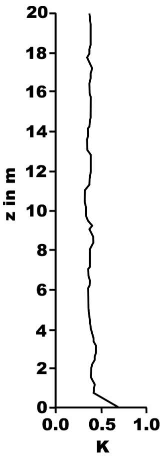


**Fig. 1.5.** Vertical temperature profile above a water surface with a molecular boundary layer, which has an linear temperature gradient (Foken *et al.* 1978)

All processes in the atmospheric boundary layer, mainly in the micrometeorological range near the ground surface (nearly neutral stratification), can be compared easily with measurements made in the laboratory (wind tunnels and water channels). Thus, the research of the hydrodynamics of boundary layers at a wall, for example by Prandtl, is applicable to atmospheric boundary layer research (Monin and Yaglom 1973, 1975; Oertel 2004; Schlichting and Gersten 2003). As will be shown in the following chapters, knowledge of micrometeorological is based to a large extent on hydrodynamic investigations. In the wind tunnel, many processes can be studied more easily than in nature. But, the reproduction of atmospheric processes in the wind tunnel also means a transformation of all the similarity numbers (see Chap. 2.1.2). Therefore, non-neutral processes can be studied in the laboratory only if extremely large temperature or density gradients can be realized in the fluid channels.

## 1.4 Energy Balance at the Earth's Surface

The earth's surface is the main energy transfer area for atmospheric processes (Fig. 1.6). It is heated by the shortwave down-welling irradiation from the sun ($K\downarrow$), and only a part of this radiation is reflected back ($K\uparrow$). Furthermore, the surface absorbs longwave down-welling radiation due to longwave emission by clouds, particles and gases ($I\downarrow$). The absorbed energy is emitted only partly into the atmosphere as longwave up-welling radiation ($I\uparrow$). In the total balance, the earth's surface receives more radiation energy than is lost, *i.e.* the net radiation at the ground surface is positive ($-Q_s^*$, see Chap. 1.4.1). The surplus of supplied energy will be transported back to the atmosphere due to two turbulent energy fluxes (see Chap. 1.4.3), the sensible heat flux ($Q_H$) and the latent heat flux ($Q_E$, evaporation). Furthermore, energy is transported into the soil due to the ground heat flux ($Q_G$) (see Chap. 1.4.2) and will be stored by plants, buildings, *etc.* ($\Delta Q_S$). The sensible heat flux is responsible for heating the atmosphere from the surface up to some 100 m during the day, except for days with strong convection. The energy balance at the earth's surface according to the law of energy conservation (see also Chap. 3.7) is:

$$-Q_s^* = Q_H + Q_E + Q_G + \Delta Q_s \tag{1.1}$$

The following convention will be applied:

Radiation and energy fluxes are positive if they transport energy away from the earth's surface (into the atmosphere or into the ground), otherwise they are negative.

The advantage of this convention is that the turbulent fluxes and the ground heat flux are positive at noon. This convention is not used in a uniform way in the literature, *e.g.* in macro-scale meteorology the opposite sign is used. Often, all upward directed fluxes are assumed as positive (Stull 1988). In this case, the ground heat flux has the opposite sign of that given above.

The components of the energy balance shown in schematic form in Fig. 1.7 are for a cloudless day with unlimited irradiation. Changing cloudiness can produce typical variations of the terms of the energy balance. The same variations occur in the case of some micrometeorological processes, which will be discussed in the following chapters. The most important variances are a positive latent heat flux after sunset and a negative sensible heat flux that begins in the early afternoon (oasis effect). A negative sensible heat flux (evaporation) is identical with dewfall. The long-term mean values of the earth's energy balance are given in Supplement 1.1. Even though the values of the radiation fluxes are high (Supplement 1.2), the energy balance with a value of 102 $Wm^{-2}$ is relatively low. The 1 K increase of the global mean temperature in the last century due to anthropogenic green house gas emissions corresponds to an additional radiation energy of 2 $Wm^{-2}$. Therefore, changes in the radiation and energy fluxes, *e.g.* due to changes in land use, can be a significant manipulation of the climate system.

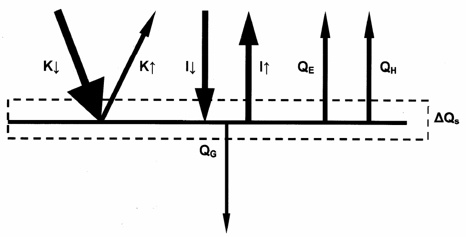


**Fig. 1.6.** Schematic diagram of the radiation and energy fluxes at the earth's surface. The net radiation according to Eq. (1.1) is the sum of the shortwave ($K$) and longwave radiation fluxes ($I$). In addition to the turbulent fluxes ($Q_H$ and $Q_E$), the energy storage $\Delta Q_s$ in the air, in the plants, and in the soil are given.

**Supplement 1.1.*** Components of the energy and radiation balance

This table gives the climatological time-average values of the components of the energy and radiation balance in W m$^{-2}$ for the whole earth (Kiehl and Trenberth 1997):

| reference level | K↓ | K↑ | I↓ | I↑ | $Q_E$ | $Q_H$ |
|---|---|---|---|---|---|---|
| upper atmosphere | –342 | 107 | 0 | 235 | 0 | 0 |
| ground surface | –198 | 30 | –324 | 390 | 78 | 24 |

**Supplement 1.2.** Energy and radiation fluxes in meteorology

Energy and radiation fluxes in meteorology are given in terms of densities. While the unit of energy is the Joule (J) and for power is Watt (W= J s$^{-1}$), the unit for the energy flux density is W m$^{-2}$. It appears that the energy flux density has *apparently* no relation to time, but the exact unit is J s$^{-1}$ m$^{-2}$. To determine the energy that one square meter gets during one hour, multiply the energy flux density by 3600 s. Energy fluxes expressed as J m$^{-2}$ are unusual in meteorology except daily sums which are given in MJ m$^{-2}$ (Mega-Joules per square meter), and sometimes kWh (kilo-Watt-hours).

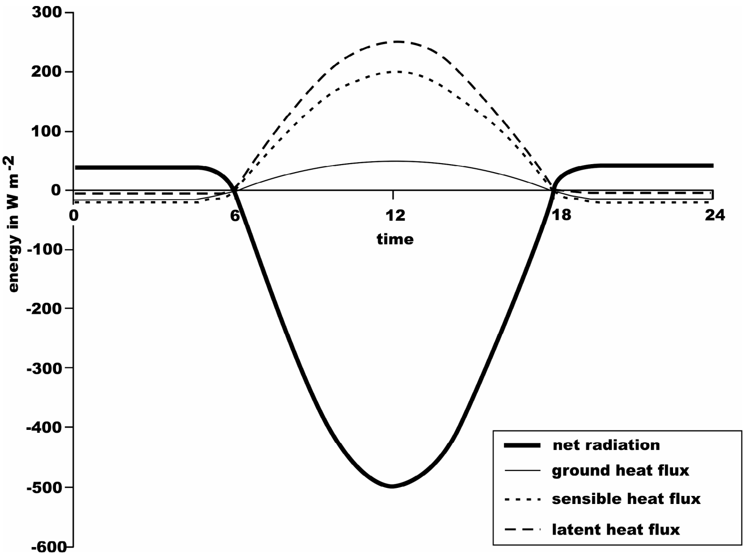


**Fig. 1.7.** Schematic of the daily cycle energy balance

* Supplements are short summaries from textbooks in meteorology and other sciences. These are included for an enhanced understanding of this book or for comparisons. For details, see the relevant textbooks.

### 1.4.1 Net Radiation at the Earth's Surface

The radiation in the atmosphere is divided into shortwave (solar) radiation and long-wave (heat) radiation. Longwave radiation has wavelengths > 3 µm (Supplement 1.3). The net radiation at the ground surface is given by:

$$Q_s^* = K\uparrow + K\downarrow + I\uparrow + I\downarrow \tag{1.2}$$

From Eq. (1.2) we see that the net radiation is the sum of the shortwave down-welling radiation mainly from the sun (global radiation), the longwave down-welling infrared (heat) radiation emitted by clouds, aerosols, and gases, the short-wave up-welling reflected (solar) radiation, and the longwave up-welling infrared (heat) radiation.  The shortwave radiation can be divided into the diffuse radiation from the sky and direct solar radiation.

Supplement 1.1 gives the climatological-averages of the magnitudes of the components of the energy and radiation balance equation. These values are based on recent measurements of the mean solar incoming shortwave radiation at the upper boundary of the atmosphere, *i.e.* $S = -1368$ Wm$^{-2}$ (Glickman 2000; Houghton *et al.* 2001) in energetic units or –1.125 Kms$^{-1}$ in kinematic units. For conversion between these units, see Chapter 2.3.1. Figure 1.8 shows the typical daily cycle of the components of the net radiation. The ratio of reflected to the incoming shortwave radiation is called the albedo:

$$a = -\frac{K\uparrow}{K\downarrow} \tag{1.3}$$

In Table 1.1 the albedos for different surfaces are given.

**Supplement 1.3.** Spectral classification of the radiation

Spectral classification of short and long wave radiation (Guderian 2000; Liou 1992)

| notation | wave length in µm | remarks |
|---|---|---|
| ultraviolet radiation | | |
| UV-C-range | 0.100–0.280 | does not penetrate the atmosphere |
| UV-B-range | 0.280–0.315 | does partly penetrate the atmosphere |
| UV-A-range | 0.315–0.400 | penetrates the atmosphere |
| visible radiation | | |
| S-A-range | 0.400–0.520 | violet to green |
| S-B-range | 0.520–0.620 | green to red |
| S-C-range | 0.620–0.760 | red |
| infrared radiation | | |
| IR-A-range | 0.76–1.4 | near infrared |
| IR-B-range | 1.4–3.0 | |
| IR-C-range | 3.0–24 | mean infrared |

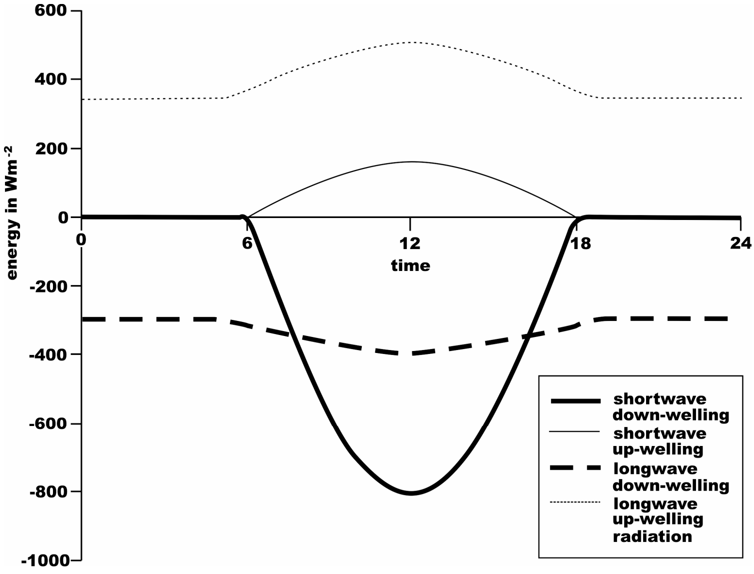


**Fig. 1.8.** Schematic of the diurnal cycle of the components of the net radiation

**Table 1.1.** Albedo of different surfaces (Geiger *et al.* 1995)

| surface | albedo |
|---|---|
| clean snow | 0.75–0.98 |
| grey soil, dry | 0.25–0.30 |
| grey soil, wet | 0.10–0.12 |
| white sand | 0.34–0.40 |
| wheat | 0.10–0.25 |
| grass | 0.18–0.20 |
| oaks | 0.18 |
| pine | 0.14 |
| water, rough, solar angle 90° | 0.13 |
| water, rough, solar angle 30° | 0.024 |

The longwave radiation fluxes will be determined according to the Stefan-Boltzmann law:

$$I = \varepsilon_{IR}\, \sigma_{SB}\, T^4 \tag{1.4}$$

where the infrared emissivities for different surfaces are given in Table 1.2, and $\sigma_{SB} = 5.67 \cdot 10^{-8}$ W m$^{-2}$ K$^{-4}$ is the Stefan-Boltzmann constant.

**Table 1.2.** Infrared emissivity of different surfaces (Geiger *et al.* 1995)

| surface | emissivity |
|---|---|
| water | 0.960 |
| fresh snow | 0.986 |
| coniferous needles | 0.971 |
| dry fine sand | 0.949 |
| wet fine sand | 0.962 |
| thick green grass | 0.986 |

In general, the up-welling longwave radiation is greater than the down-welling longwave radiation, because of the earth's surface is warmer than clouds and aerosols. It is only in the case of fog, that up-welling and down-welling radiation are equal. The down-welling radiation may be greater if clouds appear in a previously clear sky and the ground surface has cooled. For clear sky without clouds and dry air, the radiation temperature is approximately –55 °C.

Meteorological data are usually measured in UTC (Universal Time Coordinated) or in local time; however, for radiation measurements the mean or, even better, the true local time is desirable. Then, the sun is at its zenith at 12:00 true local time. Appendix A4 gives the necessary calculations and astronomical relations to determine true local time.

Measurements of global radiation are often available in meteorological networks, but other radiation components may be missing. Parameterizations of these missing components using available measurements can be helpful. However, it should be noted that such parameterizations are often based on climatological mean values, and are valid only for the places where they were developed. Their use for short-time measurements is invalid.

The possibility to parameterize radiation fluxes using cloud observations was proposed by Burridge and Gadd (1974), see Stull (1988). For shortwave radiation fluxes, the transmissivity of the atmosphere is used:

$$T_K = (0.6 + 0.2 \sin\Psi)\left(1 - 0.4\,\sigma_{c_H}\right)\left(1 - 0.7\,\sigma_{c_M}\right)\left(1 - 0.4\,\sigma_{c_L}\right) \tag{1.5}$$

For solar elevation angles $\Psi = 90°$, the transmission coefficient, $T_K$, ranges from 0.8 to 0.086. $\sigma_c$ is the cloud cover (0.0–1.0) of high clouds, $c_H$, of middle clouds, $c_M$, and $c_L$ of low clouds, (see Supplement 1.4). Notice that in meteorology the cloud cover is given in octas. (An octa is a fraction equal to one-eighth of the sky.) The incoming shortwave radiation can be calculated using the solar constant $S$:

$$K\downarrow = \begin{pmatrix} S\,T_K \sin\Psi, & \Psi \geq 0 \\ 0 & , \Psi \leq 0 \end{pmatrix} \tag{1.6}$$

**Supplement 1.4** Cloud genera

The classification of clouds is made according their genera and typical height. In the middle latitudes, high clouds are at 5–13 km a.g.l.; middle high clouds at 2–7 km a.g.l., and low clouds at 0–2 km a.g.l. The cloud heights in Polar Regions are lower while in tropical regions clouds heights can be up to 18 km.

| cloud genera | height | description |
|---|---|---|
| cirrus (Ci) | high | white, fibrously ice cloud |
| cirrocumulus (Cc) | high | small ice cloud, small fleecy cloud |
| cirrostratus(Cs) | high | white stratified ice cloud, halo |
| altocumulus (Ac) | mean | large fleecy cloud |
| altostratus (As) | mean | white-grey stratified cloud, ring |
| nimbostratus (Ns) | low | dark rain/snow cloud |
| stratocumulus (Sc) | low | grey un-uniform stratified cloud |
| stratus (St) | low | grey uniform stratified cloud |
| cumulus (Cu) | low*–mean | cumulus cloud |
| cumulonimbus (Cb) | low*–high | thundercloud, anvil cloud |

* in parameterizations classified as low clouds.

The reflected shortwave radiation can be calculated according to Eq. (1.3) by using typical values of the albedo of the underlying surface (Table 1.1). The longwave radiation balance can be parameterized using the cloud cover:

$$I^* = I\uparrow + I\downarrow = \left(0.08\,K\,m\,s^{-1}\right)\left(1 - 0.1\,\sigma_{c_H} - 0.3\,\sigma_{c_M} - 0.6\,\sigma_{c_L}\right) \tag{1.7}$$

If the surface temperature is given, then the longwave up-welling radiation can be calculated using the Stefan-Boltzmann law Eq. (1.4). The longwave down-welling radiation can be calculated using Eqs. (1.4) and (1.7).

More often, parameterizations use the duration of sunshine because it was measured for a long time in agricultural networks. Note that time series of sunshine durations are often inhomogeneous because the older Campbell-Stokes sunshine autograph was replaced by electronic methods. These parameterizations are based on climatological cloud structures and can be used only for monthly and annual averaged values, and in the region where the parameterization was developed. The parameterization is based on the well-known Ångström equation with sunshine duration, *Sd*:

$$K\downarrow = K\downarrow_{extr}\left[a + b\left(Sd/Sd_0\right)\right], \tag{1.8}$$

where constants $a$ and $b$ depend on the place of determination. For the German low lands, the constants are, for example, $a \sim 0.19$ and $b \sim 0.55$ (Wendling *et al.* 1997). The mean daily extraterrestrial incoming irradiation at the upper edge of the atmosphere can be calculated in $Wm^{-2}$ according to:

$$K\downarrow_{extr} = 28.36\left[9.9 + 7.08\,\varsigma + 0.18(\varsigma - 1)(\varphi - 51°)\right] \tag{1.9}$$

This equation is given in a form such that for a geographical latitude of $\varphi = 51°$ no correction for the latitude is necessary. The theoretical sunshine duration is the time between sunrise and sunset and expressed in hours

$$Sd_0 = 12.3 + 4.3\varsigma + 0.167\varsigma(\varphi - 51), \tag{1.10}$$

with ($DOY$= day of the year)

$$\varsigma = \sin\left[DOY(2\pi/365) - 1.39\right]. \tag{1.11}$$

Because direct measurements of the radiation components are now available, parameterizations should only be used for calculations with historical data.

### *1.4.2 Ground Heat Flux and Ground Heat Storage*

The ground surface (including plants and urban areas) is heated during the day by the incoming shortwave radiation. During the night, the surface cools due to longwave up-welling radiation, and is cooler than the air and the deeper soil layers. High gradients of temperature are observed in layers only a few millimeters thick (see Chap. 1.3). The energy surplus according to the net radiation is compensated by the turbulent sensible and latent heat fluxes and the mainly molecular ground heat flux. For the generation of latent heat flux, an energy surplus at the ground surface is necessary, and water must be transported through the capillaries and pores of the soil. Energy for the evaporation can also be provided by the soil heat flux in the upper soil layer.

In meteorology, the soil and the ground heat fluxes are often described in a very simple way, *e.g.* the large differences in the scales in the atmosphere and the soil are often not taken into account. The heterogeneity of soil properties in the scale of $10^{-3}$–$10^{-2}$ m is ignored, and the soil is assumed to be nearly homogeneous for the given meteorological scale. For more detailed investigations, soil physics textbooks must be consulted. In the following, conductive heat fluxes in the soil and latent heat fluxes in large pores are ignored.

The ground heat flux, $Q_G$, is based mainly on molecular heat transfer and is proportional to the temperature gradient times the thermal molecular conductivity $a_G$ (Table 1.3):

$$Q_G = a_G\,\frac{\partial T}{\partial z} \tag{1.12}$$

This molecular heat transfer is so weak that during the day only the upper decimeters are heated. When considering the annual cycle of ground temperature, maximum temperature is at the surface during the summer, but 10–15 m below the surface during winter (Lehmann and Kalb 1993). On a summer day, the ground heat flux is about 50–100 Wm$^{-2}$. A simple but not reliable calculation (Liebethal and Foken 2007) is: $Q_G = -0.1\,Q_s^*$ or $Q_G = 0.3\,Q_H$ (Stull 1988).

**Table 1.3.** Thermal molecular conductivity $a_G$, volumetric heat capacity $C_G$, and molecular thermal diffusivity $\nu_T$ for different soil and ground properties (Stull 1988)

| ground surface | $a_G$ in W m$^{-1}$ K$^{-1}$ | $C_G$ in $10^6$ W s m$^{-3}$ K$^{-1}$ | $\nu_T$ in $10^{-6}$ m$^2$ s$^{-1}$ |
|---|---|---|---|
| rocks (granite) | 2.73 | 2.13 | 1.28 |
| moist sand (40 %) | 2.51 | 2.76 | 0.91 |
| dry sand | 0.30 | 1.24 | 0.24 |
| sandy clay (15%) | 0.92 | 2.42 | 0.38 |
| swamp (90 % water) | 0.89 | 3.89 | 0.23 |
| old snow | 0.34 | 0.84 | 0.40 |
| new snow | 0.02 | 0.21 | 0.10 |

The determination of the ground heat flux according to Eq. (1.12) is not practicable because the temperature profile must be extrapolated to the surface to determine the partial derivative there. This can be uncertain because of the high temperature gradients near the surface (Fig. 1.9) and the difficulties in the determining thermal heat conductivity.

However, the ground heat flux at the surface can be estimated as the sum of the soil heat flux measured at some depth using soil heat flux-plates (see Chapter 6.2.6) and the heat storage in the layer between the surface and the plate:

$$Q_G(0) = Q_G(-z) + \int_{-z}^{0} \frac{\partial}{\partial t} C_G(z)\, T(z)\, dz \tag{1.13}$$

An optimal design for ground heat flux measurements was developed by Liebethal *et al.* (2005) using sensitivity analysis. According to their method, the soil heat-flux plate should be buried rather deeply (10–20cm) with some temperature measurements made above it to calculate the heat storage. A similar accuracy can be achieved if a temperature profile is used to calculate both the soil heat flux according to Eq. (1.12) at a certain depth and the heat storage between this depth and the surface.

The volumetric heat capacity $C_G = a_G / \nu_T$ ($\nu_T$ is the molecular thermal diffusivity, Table 1.3), can be assumed constant with depth in the case of uniform soil moisture. A general measurement and calculation guide for the integral of the change of the soil temperature with time is not available. Most institutes have their own schemes, not all of which are optimal solutions. The simplest method is the measurement with an integrating temperature sensor of the mean temperature of the soil layer between the surface and the heat-flux plate. For the ground heat flux near the surface, it follows that:

$$Q_G(0) = Q_G(-z) + \frac{C_G\,|\Delta z|\left[\overline{T(t_2)} - \overline{T(t_1)}\right]}{t_2 - t_1} \tag{1.14}$$

The change of the soil temperature with the time can be determined from the vertical gradient of the soil heat flux and using of Eq. (1.12):

$$\frac{\partial T}{\partial t} = \frac{1}{C_G}\frac{\partial Q_G}{\partial z} = \nu_T \frac{\partial^2 T}{\partial z^2} \tag{1.15}$$

The daily cycle of the soil temperature is to first-order a sine function (Fig. 1.10). Therefore, the surface temperature $T_s$ can be calculated depending on a temperature $T_M$, which is not affected by the daily cycle, *i.e.*

$$T_s = T_M + A_s \sin\left[\left(\frac{2\pi}{P}\right)(t - t_M)\right], \tag{1.16}$$

where $A_s$ is the amplitude and $P$ is the period of the wave of the surface temperature and $t_M$ is the time required for $T_s = T_M$ (Arya 2001).

Multiple layers are used for the modeling of the ground heat flux. Because during the daily cycle only the upper soil layers are heated (Fig. 1.10), the two-layer model (force-restore method) developed by Blackadar (1976) is widely used. The ground heat flux can be calculated from two components, *i.e.*, from the change of the temperature of the thin surface layer due to radiation and from the slow wave of the temperature difference between the surface layer and a deeper layer. The equation for the ground heat flux is (Stull 1988):

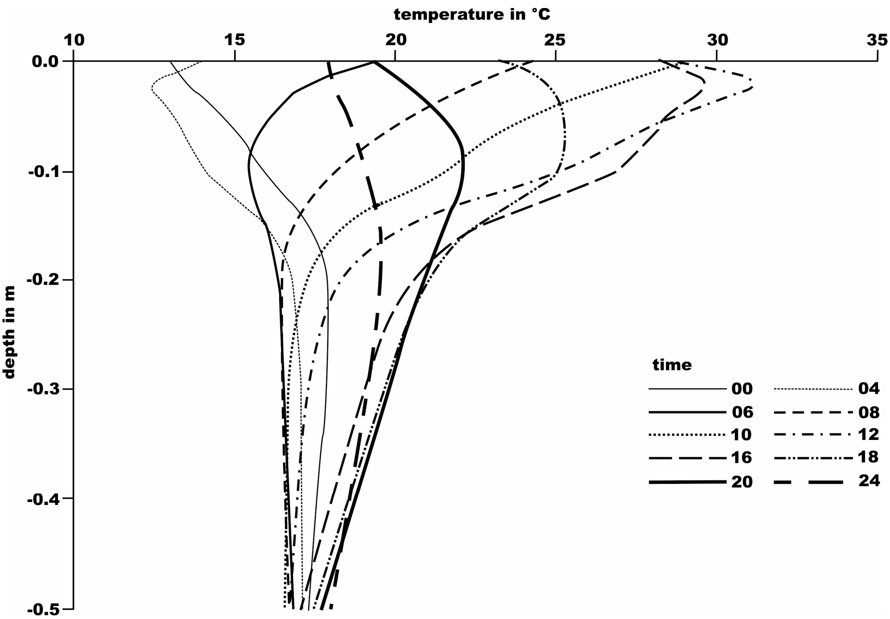


**Fig. 1.9.** Temperature profile in the upper soil layer on June 05, 1998, measured by the University of Bayreuth during the LITFASS-98 experiment (*bare soil*) at the boundary layer measuring field site of the Meteorological Observatory Lindenberg (high clouds from 12:00 to 14:00)

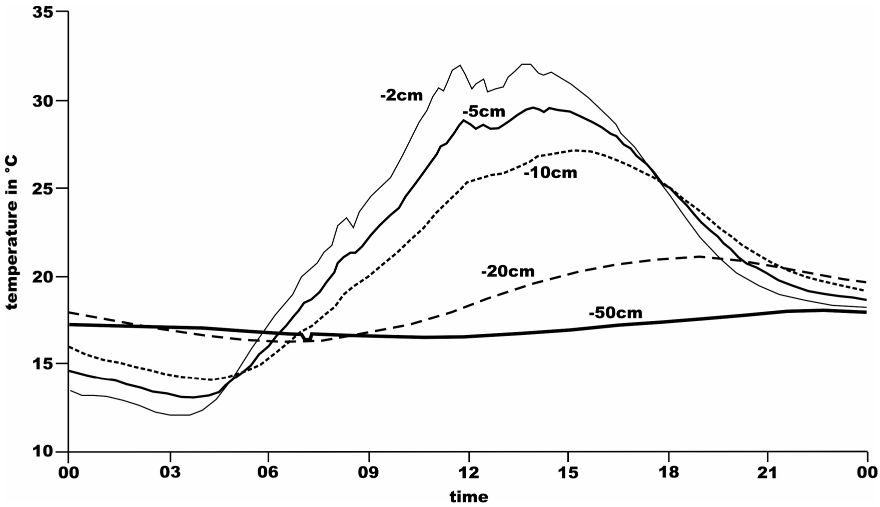


**Fig. 1.10.** Daily cycle of soil temperatures at different depth, measured by the University of Bayreuth during the LITFASS-98 experiment (*bare soil*) at the boundary layer measuring field site of the Meteorological Observatory Lindenberg (high clouds from 12:00 to 14:00)

$$Q_G = z_G\, C_G \frac{\partial T_G}{\partial t} + \left(2\pi \frac{z_G\, C_G}{P}\right)\left(T_G - T_M\right) \tag{1.17}$$

Here is $T_G$ the temperature of the upper soil layer, $T_M$ is the temperature of the deeper soil layer, $P$ is the time of the day, and $z_G$ is the thickness of the surface layer. According to Blackadar (1976), during the day $2\pi/P$ is $3 \cdot 10^{-4}$ s$^{-1}$, and at night is $1 \cdot 10^{-4}$ s$^{-1}$ (day: $T_a < T_G$, night: $T_a > T_G$, $T_a$: air temperature). The thickness of the upper soil layer depends on the depth of the daily temperature wave:

$$z_G = \sqrt{\frac{\nu_T\, P}{4\pi}} \tag{1.18}$$

This can be calculated from Eq. (1.15) using Eq. (1.16), see Arya (2001). The force-restore method has the best results in comparison to other parameterization methods (Liebethal and Foken 2007).

### *1.4.3 Turbulent Fluxes*

Contrary to the molecular heat exchange in the soil, heat exchange in the air due to turbulence is much more effective. This is because turbulent exchange occurs over scales of motions ranging from millimeters to kilometers. Turbulent elements can be thought of as air parcels with largely uniform thermodynamic characteristics. Small-scale turbulence elements join to form larger ones and so on. The largest eddies are atmospheric pressure systems. The heated turbulent elements transport their energy by their random motion. This process applies also for trace gases such as water vapor and kinetic energy. The larger turbulent elements receive their energy from the mean motion, and deliver the energy by a cascade process to smaller elements (Fig. 1.11). Small turbulent elements disappear by releasing energy (energy dissipation). On average, the transformation of kinetic energy into heat is about 2 $Wm^{-2}$, which is very small and not considered in the energy balance equation. The reason for this very effective exchange process, which is about a factor of $10^5$ greater than the molecular exchange, is the atmospheric turbulence.

Atmospheric turbulence is a specialty of the atmospheric motion consisting in the fact that air volume (much larger than molecules: turbulent elements, turbulent eddies) achieve irregular and stochastic motions around a mean state. They are of different order with characteristic extensions and lifetimes ranging from centimeters and seconds to thousands of kilometers and days.

The characteristic distribution of turbulent elements (turbulent eddies) takes place according their size and is represented by the turbulence spectrum:

The turbulence spectrum is a plot of the energy distribution of turbulent elements (turbulent eddies) according their wavelength or frequency. Depending on the frequency, the distribution is classified as macro-, meso- or micro turbulence.

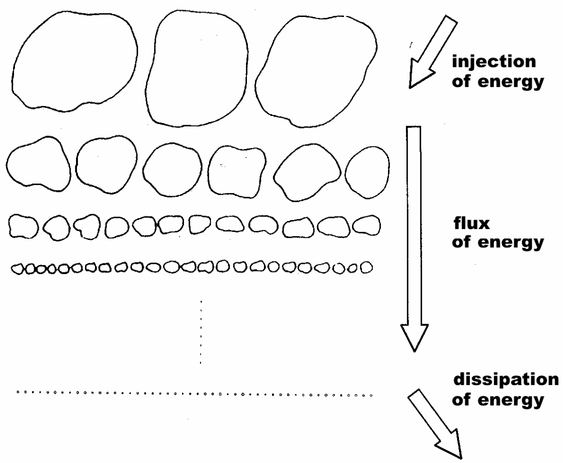


**Fig. 1.11.** Cascade process of turbulent elements (Frisch 1995), please note that the diminishing of the sizes of the elements is continuous.

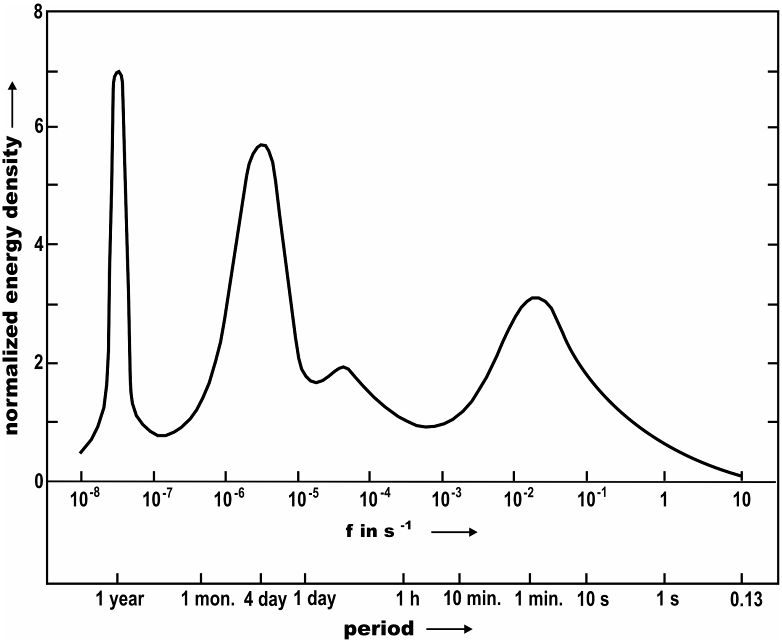


**Fig. 1.12.** Schematic plot of the turbulence spectra (Roedel 2000, modified); the range of frequencies > $10^{-3}$ Hz is called micro-turbulence

The division of atmospheric turbulence occurs over three time ranges, *i.e.* changes of high and low pressure systems within 3–6 days; the daily cycle of meteorological elements, and the transport of energy, momentum, and trace gases at frequencies ranging from 0.0001 to 10 Hz (Fig. 1.12). The transport of energy and trace gases is the main issue of micrometeorology.

Of special importance, is the inertial sub-range, which is characterized by isotropic turbulence and a constant decrease of the energy density with increasing frequency. In the range from about 0.01 to 5 Hz, no dominant direction exists for the motion of turbulent elements. The decrease of energy by the decay of larger turbulent elements into smaller ones takes place in a well-defined way according to Kolmogorov's *–5/3-law* (Kolmogorov 1941a). This law predicts that the energy density decreases by five decades when the frequency increases by three decades. The inertial sub-range merges into the dissipation range at the *Kolmogorov's microscale*. The shape of the turbulence spectra depends on the meteorological element, the thermal stratification, the height above the ground surface, and the wind velocity (see Chap. 2.5).

A typical property of turbulence, especially in the inertial sub-range, is that turbulent elements change little as they move with the mean flow. Thus, at two neighboring downwind measuring points the same turbulent structure can be observed at different times. This means that a high autocorrelation of the turbulent fluctuations exists. This is called *frozen turbulence* according to Taylor (1938).

Furthermore, the length scales of turbulent elements increase with the height above the ground surface. In an analogous way, the smallest turbulent elements with the highest frequencies are found near the ground surface. From these findings, it is reasonable to plot the turbulence spectra not as a function of frequency *f,* but as a dimensionless frequency, *n*, normalized with the wind speed *u* and the height *z*:

$$n = f\,\frac{z}{u} \tag{1.19}$$

(In the English literature, one often sees *n* as the frequency and *f* as the dimensionless frequency.)

Turbulent elements can be easily seen, *e.g.*, in plots of temperature time series with high time resolution. In Fig. 1.13, we see short-period disturbances with different intensities superposed onto longer-period (~ 60 s) disturbances. We also see that even significantly larger structures are present.

The calculation of the heat fluxes (sensible and latent) caused by turbulent elements is analogous to Eq. (1.12) using the vertical gradients of temperature *T* and specific humidity *q* (see Supplement 2.1), respectively. However, the molecular transfer coefficient must be replaced by the turbulent diffusion coefficient. The sensible heat flux, $Q_H$, describes the turbulent transport of heat from and to the earth's surface. The latent heat flux, $Q_E$, describes the vertical transport of water vapor and the heat required for evaporation at the ground surface. This heat will be deposited later in the atmosphere when condensation occurs, *e.g.* in clouds. The relevant equations are:

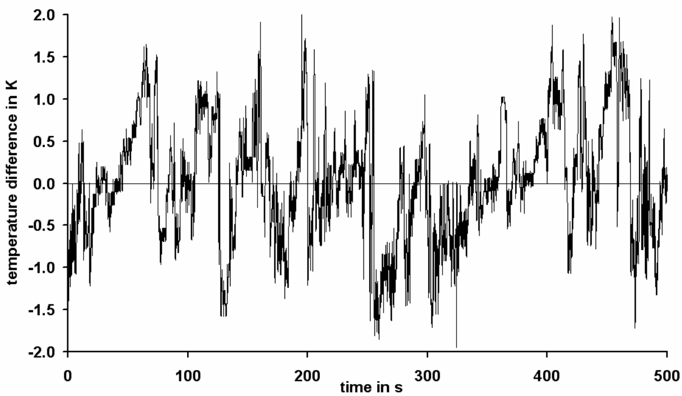


**Fig. 1.13.** Time series of the air temperature above a spruce forest (University of Bayreuth, Waldstein/Weidenbrunnen site), August 19, 1999, 11:51–12:00 UTC, 500 s measuring period (Wichura *et al.* 2001)

$$Q_H = -\rho\, c_p\, K_H \frac{\partial T}{\partial z}, \tag{1.20}$$

$$Q_E = -\rho\, \lambda\, K_E \frac{\partial q}{\partial z} \tag{1.21}$$

with the air density $\rho$, the specific heat for constant pressure $c_p$, and evaporation heat of water $\lambda$. The turbulent diffusion coefficients $K_H$ and $K_E$ are normally complicated functions of the wind speed, the stratification, and the properties of the underlying surface. Their evaluation is a special issue of micrometeorology. In Chap. 2.3, several possible calculations of the diffusion coefficients are discussed. Also common is the *Austausch coefficient* (Schmidt 1925), which is the product of the diffusion coefficient and the air density:

$$A = \rho\, K \tag{1.22}$$

An example of the daily cycle of the turbulent fluxes including the net radiation and the ground heat flux is shown in Fig. 1.14. It is obvious that during the night all fluxes have the opposite sign to that during the day, but the absolute values are much less. After sunrise, the signs change and the turbulent fluxes increase rapidly. The time shift between the irradiation and the beginning of turbulence is only a few minutes (Foken *et al.* 2001). The time shift of the ground heat flux depends on the depth of the soil layer. The maximum of the turbulent fluxes on clear days occurs shortly after midday.

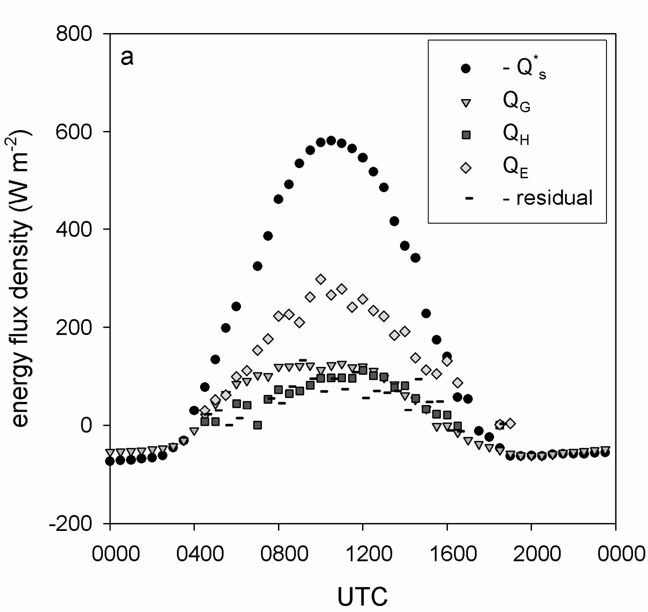


**Fig. 1.14.** Typical daily cycle of the components of the energy balance measured above a corn field on June 07, 2003 during the experiment LITFASS–2003 (Mauder *et al.* 2006)

In the case of optimal conditions for evaporation, *i.e.* high soil moisture and strong winds, the evaporation process will be greater than the sensible heat flux, if not enough radiation is available. In such cases, the sensible heat flux changes its sign 1–3 hours before sunset, and sometimes shortly after noon. This case is called the "oasis effect", and is also found in the temperate latitudes. The latent heat flux has also large values after sunrise, and changes sign after midnight (dewfall). From Fig. 1.14, it is obvious that using measured values the energy balance according to Eq. (1.1) is not closed. The missing value is called the residual. This very complex problem is discussed in Chap. 3.7.

While over land in the temperate latitudes the sensible and latent heat fluxes are of the same order, over the ocean the evaporation is much greater. In some climate regions and under extreme weather conditions, significant deviations are possible.

## 1.5 Water Balance Equation

The energy balance Eq. (1.1) is connected to the evaporation through the water balance equation:

$$0 = N - Q_E - A \pm \Delta S_W \,, \tag{1.23}$$

**Supplement 1.5.** Water cycle of Germany

Mean annual data of the water cycle of Germany (Source: German Meteorological Service, Hydrometeorology) in mm (1 mm = 1 L m$^{-2}$)

| precipitation | | evaporation | |
|---|---|---|---|
| 779 mm | | 463 mm | |
| into evaporation | 463 mm | from transpiration | 328 mm |
| into ground water | 194 mm | from interception | 72 mm |
| into runoff | 122 mm | from soil evaporation | 42 mm |
| | | from surface water evaporation | 11 mm |
| | | from service water evaporation | 11 mm |

**Supplement 1.6.** Water cycle of the earth

Mean water balance of the earth in $10^3$ km$^3$ a$^{-1}$ (Houghton 1997)

| surface | precipitation | evaporation | runoff |
|---|---|---|---|
| land surface | 111 | 71 | 40 |
| ocean surface | 385 | 425 | 40* |

* water vapor transport in the atmosphere from the ocean to the land, for instance as cloud water

where $N$ is the precipitation, $A$ the runoff, and $\Delta S_W$ the sum of the water storage in the soil and ground water. Evaporation is often divided into the physically-caused part, the *evaporation*, which is dependent on the availability of water, the energy input, and the intensity of the turbulent exchange process; and the *transpiration* which is caused by plant-physiology, the water vapor saturation deficit, and the photosynthetic active radiation. The sum of both forms is called *evapotranspiration*. Evaporation occurs on the ground, on water surfaces, and on wetted plant surfaces. The latter is the evaporation of precipitation water held back at plant surfaces (interception). Micrometeorology plays an important role for the determination of evapotranspiration and the investigation of the water cycle (Supplement 1.5, Supplement 1.6). Data show that the precipitation-evaporation cycle over the land is not as strongly coupled as they are over the ocean.

The water balance equation is widely used in hydrological investigations. There, the evaporation connects meteorology with hydrology. This field of investigations is often called hydrometeorology.

http://www.springer.com/978-3-540-74665-2

Micrometeorology
Foken, Th.
2008, XX, 308 p. 113 illus., Softcover
ISBN: 978-3-540-74665-2